Lerdprom, W.; Zapata-Solvas, E.; Jayaseelan, DD.; Borrell Tomás, MA.; Salvador Moya, MD.; Lee, WE. (2017). Impact of microwave processing on porcelain microstructure. Ceramics International. 43(16):13765-13771. https://doi.org/10.1016/j.ceramint.2017.07.090

Impact of Microwave Processing on Porcelain Microstructure

Wirat Lerdprom [1], Eugenio Zapata-Solvas [1], Doni. D. Jayaseelan [2],

Amparo Borrell [3,] Maria. D. Salvador [3] and William. E. Lee[1]

[1] Department of Materials, Imperial College London, South Kensington Campus, London, SW7 2AZ, UK

[2] Department of Mechanical and Aerospace Engineering, Kingston University London, Kingston upon Thames Surrey, KT1 1LQ, UK

[3] Instituto de Tecnología de Materiales (ITM), Universitat Politècnica de València, Camino de Vera, s/n, 46022 Valencia, Spain

Abstract

Microstructural evolution on sintering of porcelain powder compacts using microwave radiation was compared with that in conventionally sintered samples. Using microwaves sintering temperature was reduced by ~ 200 °C and dwell time from 15 min to 5 min while retaining comparable physical properties i.e. apparent bulk density, water absorption to conventionally sintered porcelain. Porcelain powder absorbed microwave energy above 600 °C due to a rapid increase in its loss tangent. Mullite and glass were used as indicators of the microwave effect: mullite produced using microwaves has a nanofibre morphology with high aspect ratio (~32±3:1) believed associated with a vapour-liquid-solid (VLS) formation mechanism not previously reported. Microwaves also produced mullite with different chemistry having ~63 mol% alumina content compared to ~60 mol% alumina in conventional sintered porcelain. This is likely due to accelerated Al^{+3} diffusion in mullite under microwave radiation. Liquid glass was observed to form at relatively low temperature (~800 °C) using microwaves when compared to conventional sintering which promoted the porcelains ability to absorb them.

Keywords,

Porcelain, Aluminosilicate, Mullite, Microwave sintering, Loss tangent, Field assisted sintering technique

I. Introduction

Use of microwaves for material processing has accelerated in recent years because they provide a promising alternative energy source potentially reducing total energy consumption [1-3]. Microwaves are absorbed directly in bulk material allowing volumetric heating and inducing enhanced diffusion rates [2]. Microwave energy sometimes so called microwave effect which is a non-thermal process to heat materials. The materials are heated via rotation under the field and lose their energy by collisions. It is also a selective heating process so that almost all microwaves are converted to energy. Since it is volumetric heating, the temperature profile in the sample bulk is inverse (inside is hotter than surface); thus a potential drawback of microwave heating, in samples with low thermal conductivity, is the 'thermal runaway effect' (an uncontrolled temperature rise); and where the surface temperature is significantly lower than the interior temperature. Thermal runaway may lead to non-uniform microstructure or localised melting [4, 5] but can be mitigated by use of microwave heating associating with conventional firing process so called hybrid microwave heating which leads to a minimal temperature gradient throughout a sample [6, 7].

The successful application of microwave sintering depends on the dielectric properties of the materials—mainly dielectric constant, dielectric loss, loss tangent and penetration depth—at the microwave frequency (2.45 GHz is typically used for materials processing). The dielectric constant ($\boldsymbol{\varepsilon}'$) defines the ability of ions and dipole to reorient under an alternating electric field while dielectric loss (ε'') represents heat generation during material coupling with the alternating electric field. Both values are used to calculate how much heat is generated in the material by the microwaves in the loss tangent ($\tan\delta$). The penetration depth (D_p) is defined as the distance over which the intensity of the electromagnetic fields decays to 1/e. Generally, loss tangents ranging from 0.01-1 are suitable for microwave processing [8]. Furthermore, dielectric properties of most materials change with temperature, at high temperature absorbing more microwave energy. These changes of dielectric properties may also lead to thermal runaway.

Porcelains and the raw materials from which they are made, are poorly microwave absorbing materials, all of which do not couple well with microwaves at room temperature although they can effectively absorb microwaves above a critical

temperature [9, 10], making it possible to process porcelains using microwaves at elevated temperature. Generally, porcelains are vitreous ceramics derived from triaxial mixtures of clay minerals, feldspar flux and quartz filler. After heat treatment, fired porcelains comprise mullite, glass and residual quartz [11-13]. Several chemical reactions occur during porcelain firing including dehydroxylation of the clay from ~ 450-600 °C, glass formation by feldspar melting at ~990-1050 °C (depending on its chemistry), and partial quartz dissolution >1200 °C [11, 13]. Mullite starts to form around 940-980 °C and different types of mullite are observed depending on sources; primary mullite forms by the clay decomposition and found in the clay relicts while secondary mullite forms from the reaction of the clay and flux melt, and found in the glass region [12, 14]. These transformations also change the dielectric properties of the porcelain being fired affecting its microwave absorbability.

Use of microwave energy to sinter porcelains has been reported. *Menezes et al*.[15] successfully produced different porcelain bodies including sanitary ware, dental and electrical porcelains using a 2.45 GHz hybrid microwave sintering system (also using infrared heat and a susceptor). Water absorption was at the same level as in conventionally sintered porcelain, but the maturing temperature of microwave sintering was higher ~20 °C compared with the conventional one. However, substantial (6 folds) reduction of dwell time was observed with microwave sintering, a significant advantage. All bodies microwave sintered exhibited higher density. Microwave sintering of high voltage porcelain insulators [16] revealed better properties (density, modulus of rupture, and dielectric strength) compared to conventional sintered at the same maturing temperature, and the firing time was reduced ~80%.

Shawn [17] successfully produced a large-cross section (12 cm of diameter) electrical porcelain insulator using Microwave Assisted Technology (MAT), a combination of electric furnace and microwave heating, with 5 times shorter processing time compared to the conventional process.

Santos et al.,[18] developed a multimode cavity (2.45 GHz) microwave oven which is capable of firing porcelain tableware with a SiC slab as a support, not susceptor. The microwave sintered porcelain showed similar impact resistance, porosity, water absorption, and phase composition to conventionally sintered porcelain. The sintering process was faster resulting in lower processing costs. An important aspect of this study was the microwave power distribution which played an important role in conferring homogeneity on the sample. A critical problem in

microwave sintering is thermal runaway due to inhomogeneous microwave absorption. To combat this *Monteiro et al.*,[19] developed a control system which creates a uniform electromagnetic field and therefore more uniform heating, even at high heating rates. While there have been several studies dealing with the microwave sintering of porcelains, none have reported in detail the effect of microwave heating on microstructural evolution, thus in the present study the effect of microwave radiation on mullite formation, and porcelain densification will be discussed.

II. Experimental

The raw material used in this work was spray dried porcelain powder provided by a tile manufacturer, used in as-received form without any reprocessing consisting of kaolinite, albite and quartz. The powder was uniaxially cold-pressed using 35 MPa into 13 mm diameter and 7 mm thick pellets in a steel die. The pellets were dried overnight at 110 °C and stored in an oven until further experiments.

Thermal behaviour of the spray dried powder, with mean particle size (D_{50}) of 10 µm, was characterised by using a simultaneous thermogravimetry-differential thermal analyzer (TG-DTA, Netzsch STA 449C, Jupiter, Selb, Germany) under continuous air flow at a rate of 50 ml/h from 25-1200 °C at a heating rate of 10 °C/min and instrument cooling rate.

The pellets were sintered under air in a single mode cylindrical microwave cavity operating in the TE_{111} mode with a resonant frequency of 2.45 GHz [20]—a quartz tube was used as sample holder (Fig.1a). The furnace E-field has maximum (E_r and E_φ components) in the center, where the samples are located [21]. The final temperatures reached were 850, 900, 1000 and 1100 °C using a heating rate of ~30 °C/min with 5 min of holding time at the maximum temperatures.

Initially, pellets were exposed to the microwaves with neither insulation nor susceptor used. As a result, they were not sintered uniformly. A small well-sintered region (~4 mm^3) in the middle of the sample indicated a need to modify the setup as presented in Fig.1b. Finally, silicon carbide powder as susceptor and alumina insulation were used to promote uniform temperature distribution (Fig.1b). The temperature of the sample was monitored using an infrared radiation thermometer (Optris CT-Laser LT, 8–14 µm), focused on the sample surface. For comparison, the same porcelain pellets were conventionally sintered at 850, 900, 1000, 1100, 1175 and 1200 °C using a heating rate of 10 °C/min with 15 min hold at each temperature.

Apparent bulk density (ABD) and water absorption (WA) of dense samples were obtained using an ASTM standard (C20-00) immersion method. Phase analyses of the sintered samples were carried out using X-ray diffraction (XRD, Bruker D2 Phaser, Madison, WI, USA). XRD data were collected from 15° to 65° 2θ with CuK_α radiation (λ=0.154 nm) at 30kV and 10 mA with a step size of 0.03° and a count time of 1 s. Diffraction patterns were analyzed using commercial software (X'pert high score plus software, Pan Analytical). Mullite chemistry was calculated

from the XRD line broadening using Ban and Okada equation [25]. Microstructures were examined using a scanning electron microscope, SEM, (Auriga: Carl Zeiss; Oberkochen, Germany) at an accelerating voltage of 5 kV, under high vacuum mode and using secondary electron imaging (SEI).

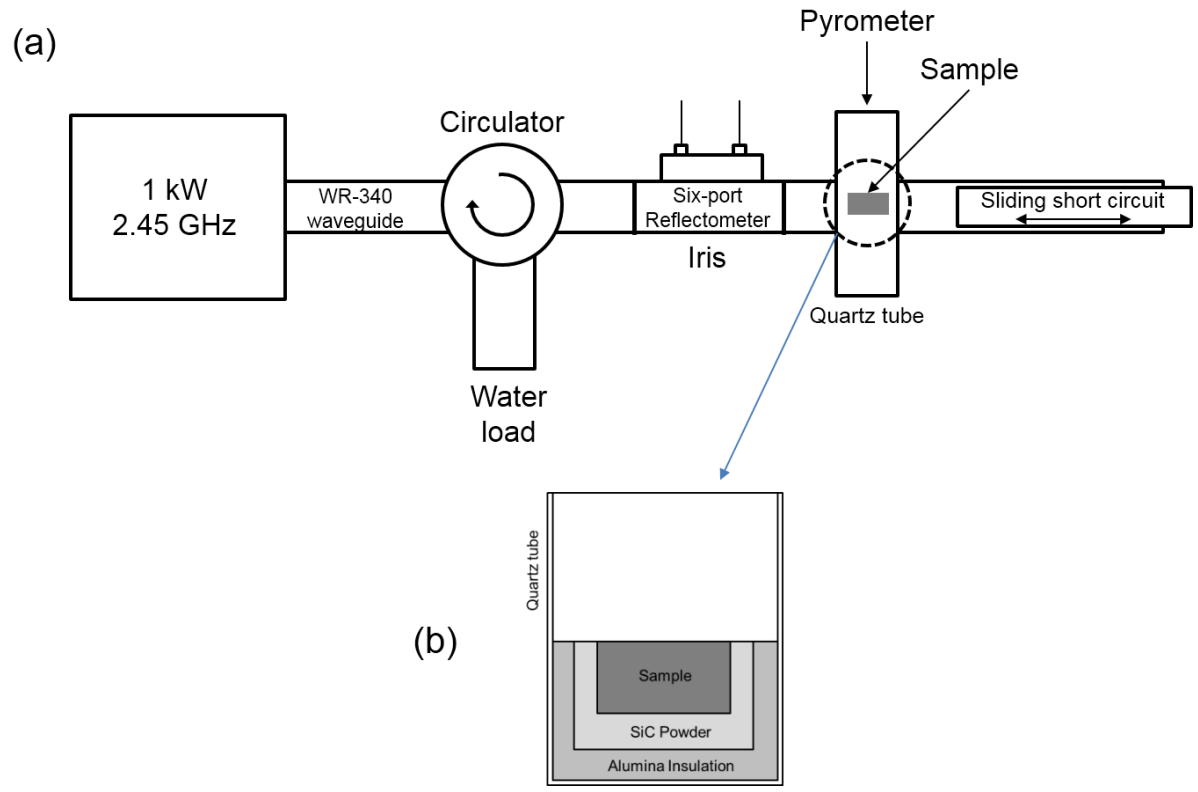

Fig.1 a) Schematic view of the microwave sintering cavity, b) the sample environment in the microwave cavity.

III. Results and discussion

Fig.2 shows development of ABD and WA as a function of sintering temperature for conventionally and microwave sintered samples. Densification of the porcelain using microwave energy started at relatively low temperature (~800 °C) compared with samples fired in the absence of microwave radiation, which started to densify at ~1100 °C. Conventionally sintered samples reached their maximum ABD (2.40 g/cm^3) after firing at 1175 °C whereas the microwave sintered sample reached its maximum ABD (2.36 g/cm^3) at 1000 °C, beyond these temperatures the ABD decreased. The WA of the samples sintered using microwave was lower than the conventionally sintered samples from 850-1100 °C indicating these samples had better degree of densification, but once the samples reached their maximum ABD, conventionally sintered samples had WA of 0.1% while microwave sintered samples had WA of 0.8%. The difference of maximum ABD and WA resulted from the different microstructure of the samples as shown in Fig.3. Furthermore, increasing WA associated with decreasing ABD was due to a bloating effect which is a common phenomenon when porcelains are fired beyond the optimal temperature [12-14].

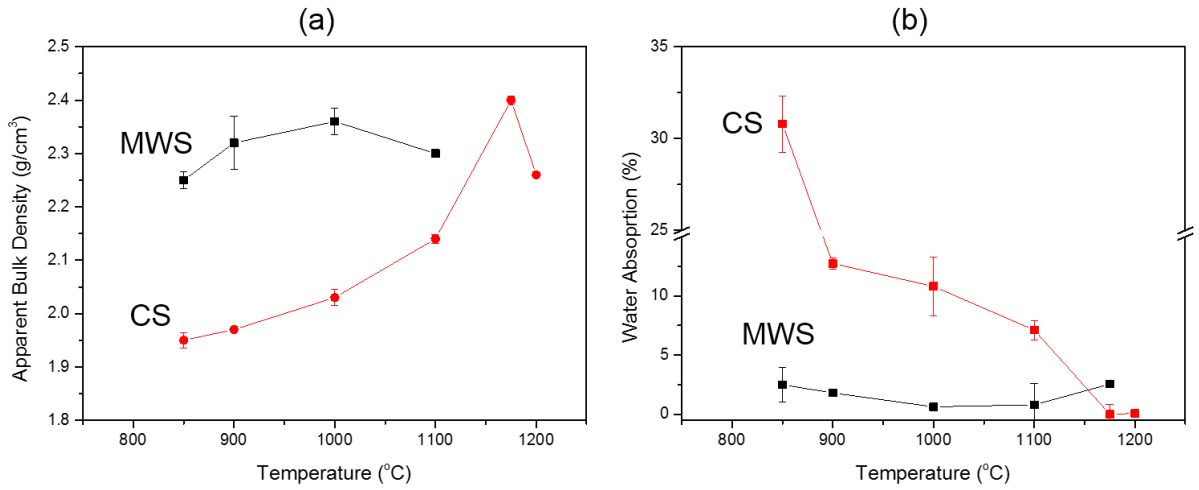

Fig.2 a) ABD and b) WA of conventionally (CS) and microwave sintered (MWS) porcelains as a function of temperature. Note that 10°C/min and 15 min dwell were used in CS while 30°C/min and 5 min dwell were used in MWS.

Fig.3a compares the thermal profile of the fully sintered porcelain samples sintered using conventional (10 °C/min, 1175 °C, 15 min dwell) and microwave (30 °C/min, 1000 °C, 5 min dwell) processes. Excluding the cooling step, the densification took 3 times shorter by microwave processing to produce fully dense sample compared to the CS process. SEI (Fig.3b) reveals distinct microstructures;

CS samples were dense with small pores (<30 μm of diameter) whereas MWS samples contained large pores (>300 μm of diameter) due to over firing. The craters (large pores) in the MWS samples arose from liquid generated by microwave radiation likely from a combination of two factors. First, the interior temperature produced was higher than at the surface temperature since the temperature was monitored at the surface (pyrometer). Second, melting feldspar produced liquid so changing the sample dielectric properties [23] , so that the sample absorbed more microwave energy, thus the temperature rose uncontrollably.

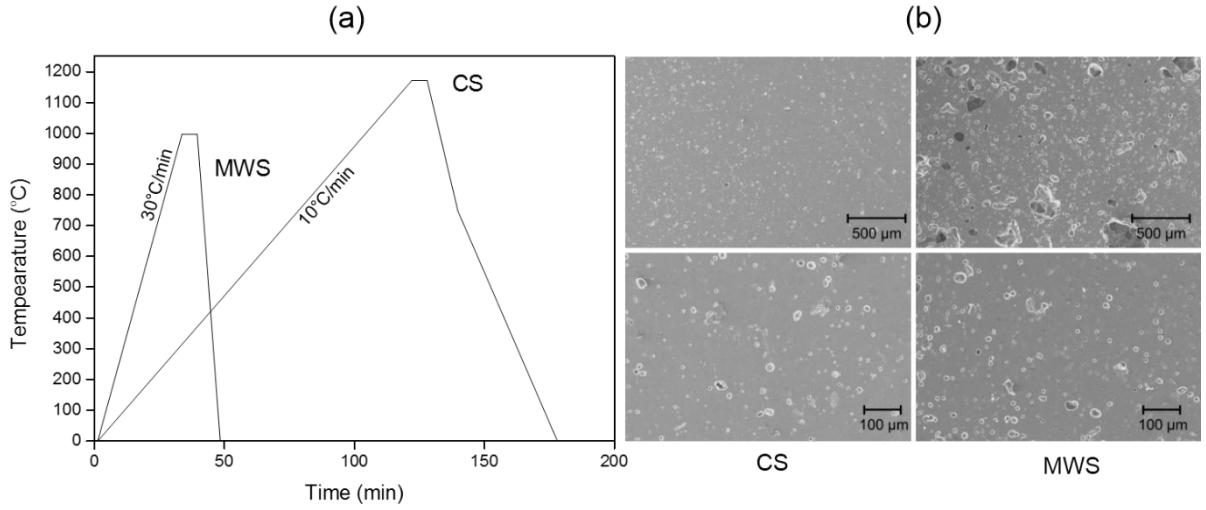

Fig.3 a) Sintering curves of conventional and microwave heat treatments, b) SEM images of conventionally sintered (CS) and microwave sintered (MWS) porcelain samples.

The thermal behaviour of the green porcelain powder conventionally sintered (Fig.4) reveals total weight loss ~5%, 1% from physically-bound evaporation, and 4% from chemically-bound water decomposition from the clays. The two large endothermic peaks arose from evaporation of physically-bound water at 100-200 °C and dehydroxylation of chemically-bound water of the clay between 450-600 °C. However, the endothermic peak of the α-β quartz inversion at 573 °C was masked by overlap with the clay dehydroxylation peak. The small exothermic peak around ~940 °C suggested initial formation of the spinel-alumina phase from the clay species [11-14, 28, 29]. This thermal behaviour implied that changing thermal behaviour of the powder at elevated temperature changed its ability to absorb microwaves. Fig.5 shows dielectric behaviour of the porcelain sample under alternating electric field of 1 MHz. Fig.5a was the calculated loss tangent of the porcelain powder from room temperature to 900 °C using $tan\,\delta = \sigma/2\pi f\varepsilon_0$, where σ is overall electrical

conductivity, *f* is frequency of alternating electric field, and ε_0 is permittivity of free space (ε_0 = 8.85x10^{-12} F·m^{-1}).

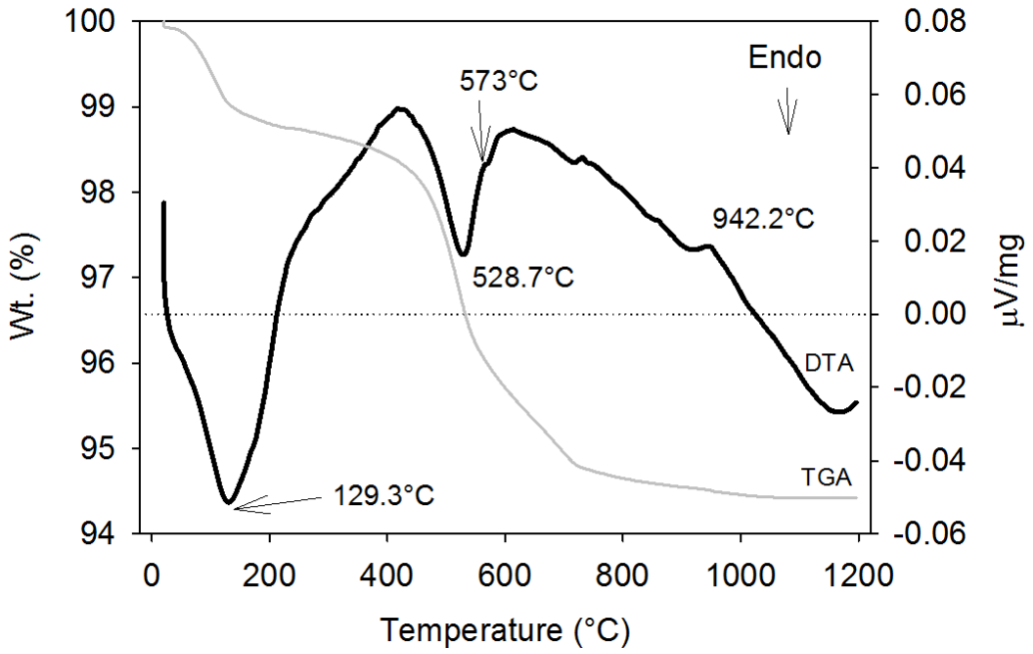

Fig.4. Thermal behaviour (TGA and DTA) of CS porcelain spray dried powder.

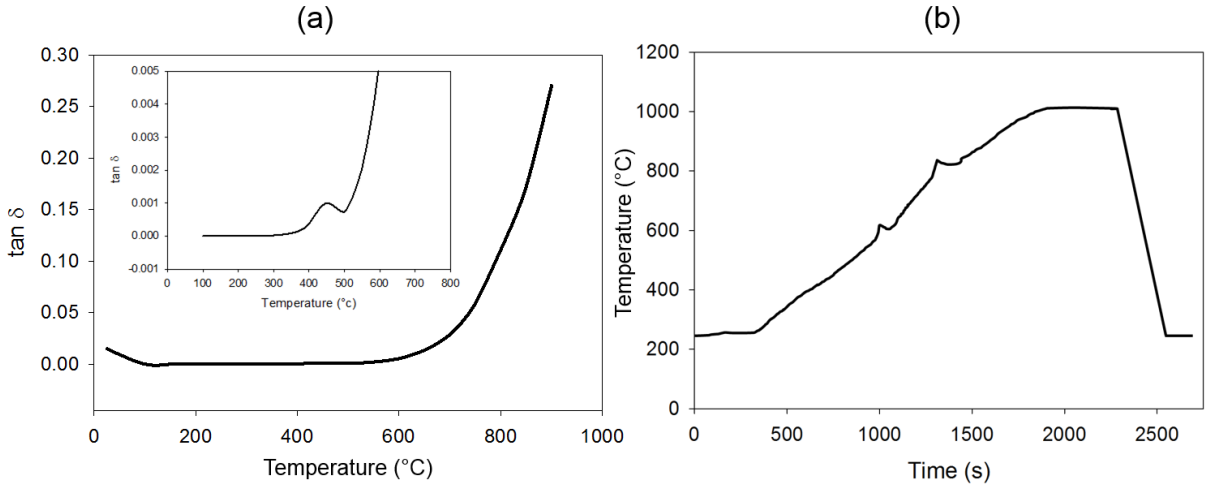

Fig.5. (a) Calculated loss tangent (tan δ) of the porcelain sample as a function temperature, the inset shows detail at 400-500°C, and (b) the temperature profile showing 2 humps at 600 and 800°C corresponding to the rapid change of the tan δ.

Generally, microwave energy is effectively absorbed at 0.01-5 [4] of loss tangent. In this study, the porcelain sample did not absorb microwave energy well from 100-600 °C since its loss tangent was low (<0.001), meaning that sample temperature increased slowly from room temperature until ~ 600°C. Above 600°C, the loss tangent increased exponentially rapidly elevating sample temperature

(indicated by the peak ~ 600 °C in Fig.5b). The second peak at 800 °C in Fig.5b is attributed to strong microwave absorbtion due to increasing loss tangent due to liquid formation from albite melting.

Microwave energy thus produced dense porcelains with promising physical properties at low temperature and short dwell time compared with the conventional sintering process. Change of sample loss tangent played an important role in the microwave absorbability and temperature increase. Liquid formation (albite melt) contributed most to the densification of porcelains since it quickly changed the loss tangent. Porcelain samples could be heated from room temperature in a microwave single mode cavity but to produce homogeneous samples insulation and susceptor were required.

In this work, only fully dense CS and MWS samples were used to study the effect of microwaves on microstructural changes (Fig. 6). The low magnification SEI images (Fig. 6a, c) reveal microstructures containing mullite, quartz, and glassy phase. CS samples were dense containing mullite and partially dissolved quartz in the glass matrix while MWS samples contained networks of mullite needles grown in the glass matrix. High magnification SEI images (Fig. 6b,d) reveal distinctive mullite morphologies. Mullite crystals in CS samples were 71(±11) nm thick whereas in MWS samples they were 56(±9) nm thick (Fig. 7a). CS samples, however, contained low aspect ratio mullite needles (~9±2:1) while MWS produced fibre-like mullite with high aspect ratio (~32±3:1) (Fig. 7b).

Mullite in porcelains can be differentiated by its aspect ratio. Iqbal and Lee proposed a notation considering the aspect ratio in which type I mullite (primary mullite) exhibits low aspect ratio (1-3:1), type II (secondary mullite) has aspect ratio of 3-10:1, and type III (secondary mullite) possesses very high aspect ratio (>30:1) [12]. Thus, the mullite formed in this porcelain via MWS is type III and via CS is type II.

Mullite crystallite size was also investigated via XRD using the Scherer's equation for the (110) plane peaks. Calculating the full width half maximum (FWHM) indicates the average mullite crystallite size of CS samples was ~39(±3) nm while from MWS it was ~28(±3) nm. While the mullite crystal sizes from SEM and XRD differed this may arise from the different sampling volumes of each technique, nonetheless the trends were the same.

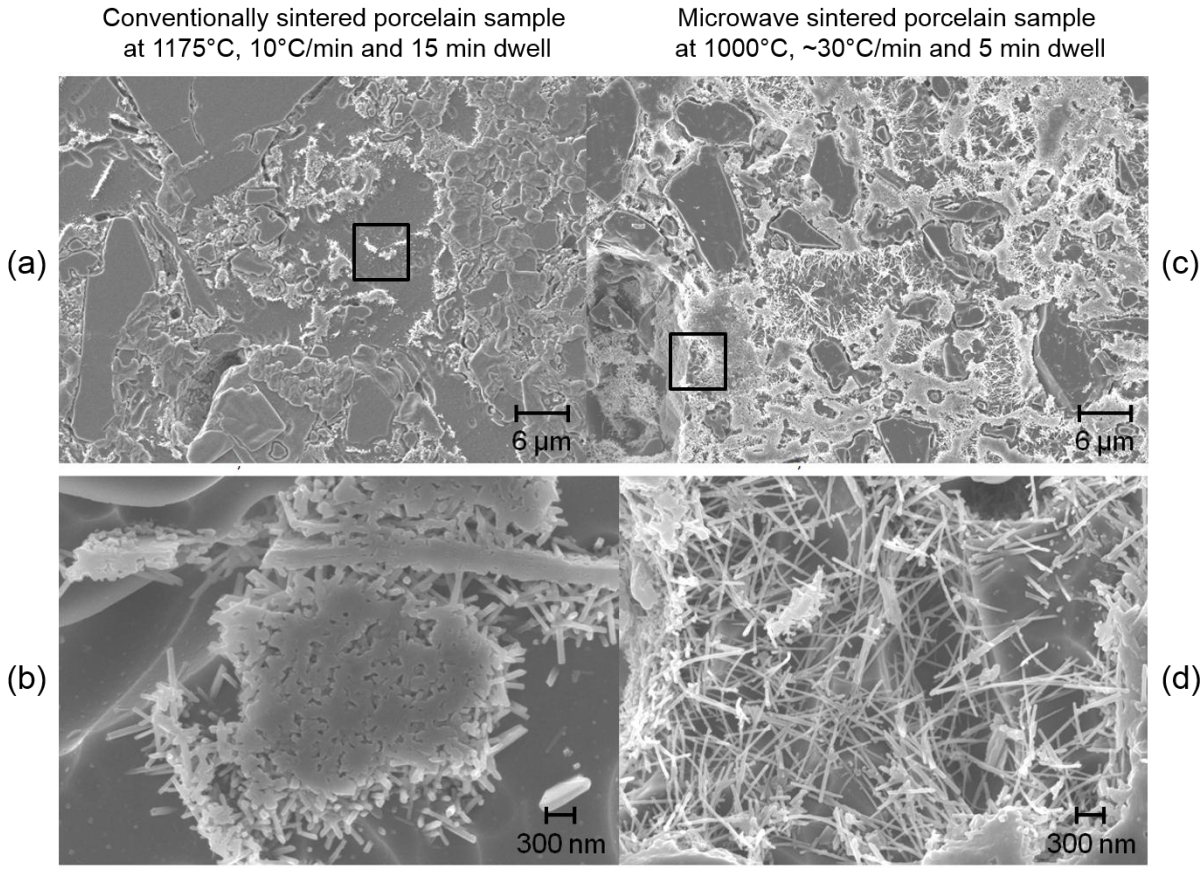

Fig.6. SEI images of CS and MWS porcelain samples, a) and c) low magnification images showing overall phase content, and b) and d) high magnification images showing the distinctive mullite morphologies.

Mullite usually has acicular morphology with the long fibre axis being the crystal c-axis [24]; the c-axis has higher free energy than those in the [hk0] directions. Fig. 8a reveals an unusual mullite morphology growing inside a bubble in a MWS sample. Mullite in the bubbles is believed to grow via a Vapour-Liquid-Solid (VLS) mechanism [30, 31]. Mullite then continually grew in [001] direction in to the air which had nuclei randomly precipitated on the needles (Fig. 8b-c). These nuclei may assist the growth of high aspect ratio needles. This feature was not observed in CS samples. Also, the formation of mullite via VSL had been not reported in conventional sintering of porcelain.

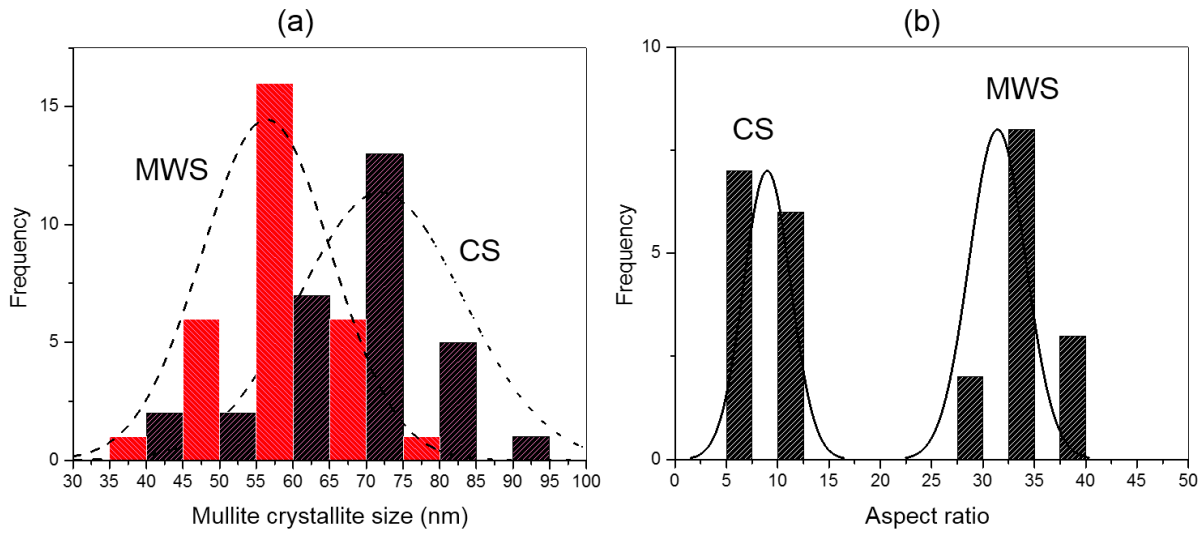

Fig. 7. Histograms present (a) crystallite size, and (b) aspect ratio of mullite formed in the porcelain samples under conventional and microwave sintering using SEM.

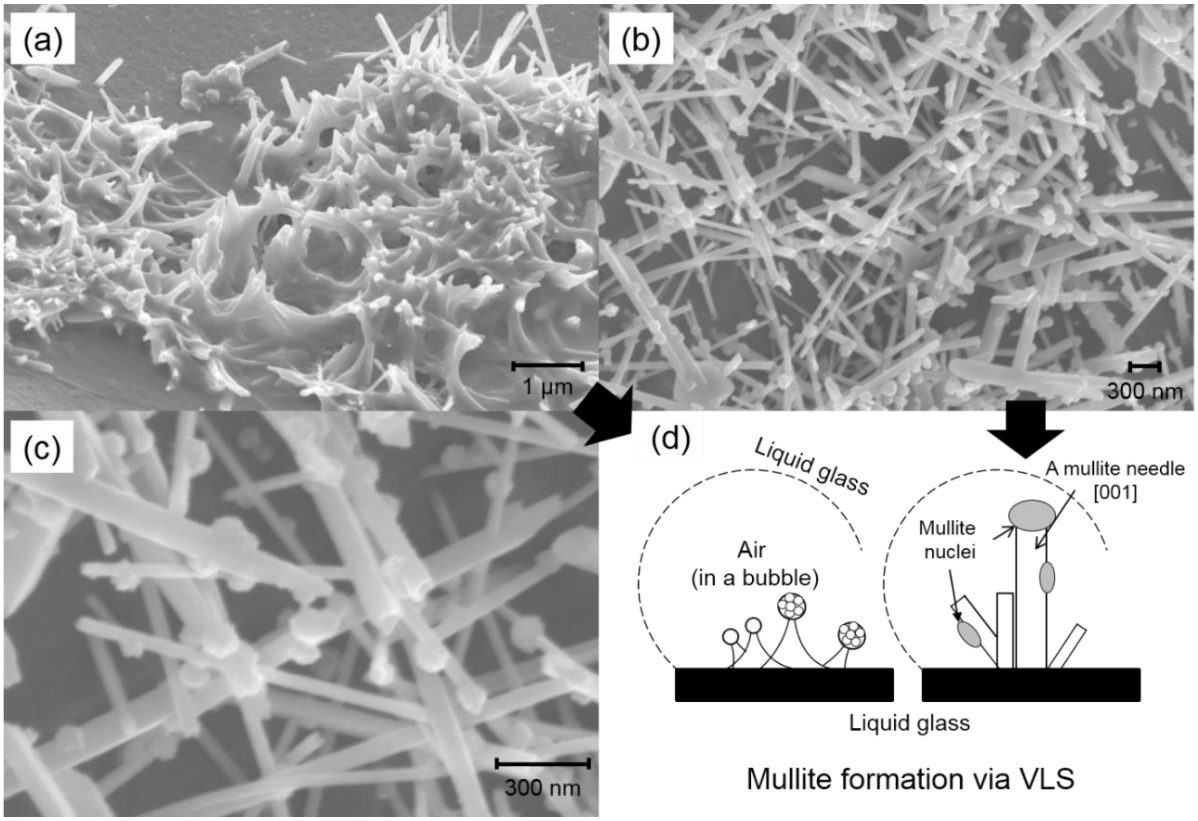

Fig.8 Vapour-Liquid-Solid growth mechanisms of mullite needles under microwave radiation: (a) mullite initially formed in a bubble surrounded by liquid glass phase, (b) mullite needles further grow in bubbles, (c) mullite nuclei precipitated on the mullite needles, and (d) the cartoon diagram showing the growth mechanism.

XRD (Fig. 9), reveals MWS samples show larger mullite integrated peak areas suggesting that mullite in this sample formed more than that in the CS

samples in agreement with the SEI of Fig. 6. CS samples contained smaller peaks of residual albite not observed in MW samples.

Chemistry of mullite was calculated using the method of Ban and Okada [25] showing molar percent of alumina in mullite. MWS sample mullite had ~63 mol% of alumina compared to ~60 mol% alumina in CS mullite. However, the crystal structures of the mullite in both samples were orthorhombic rather than tetragonal as indicated by the split of (120) and (210) XRD peaks (Fig. 9). The reason why the mullites had different alumina contents may be explained by the effect of the microwave radiation. Formation of MWS mullite was accelerated by reduction of the reaction barriers of Al^{+3} ions diffusion in the mullite structure [26] which can also be deduced from its fibrous morphology. Moreover, since the liquid glass formed earlier in MWS samples so that the mullite crystals had more time to grow and accommodate alumina into their structures. Thus, MWS mullite had alumina content more than its stoichiometry. Another possibility was the temperature of mullite formation under microwave might be too low to obtain the stoichiometric mullite (60 mol%) [27].

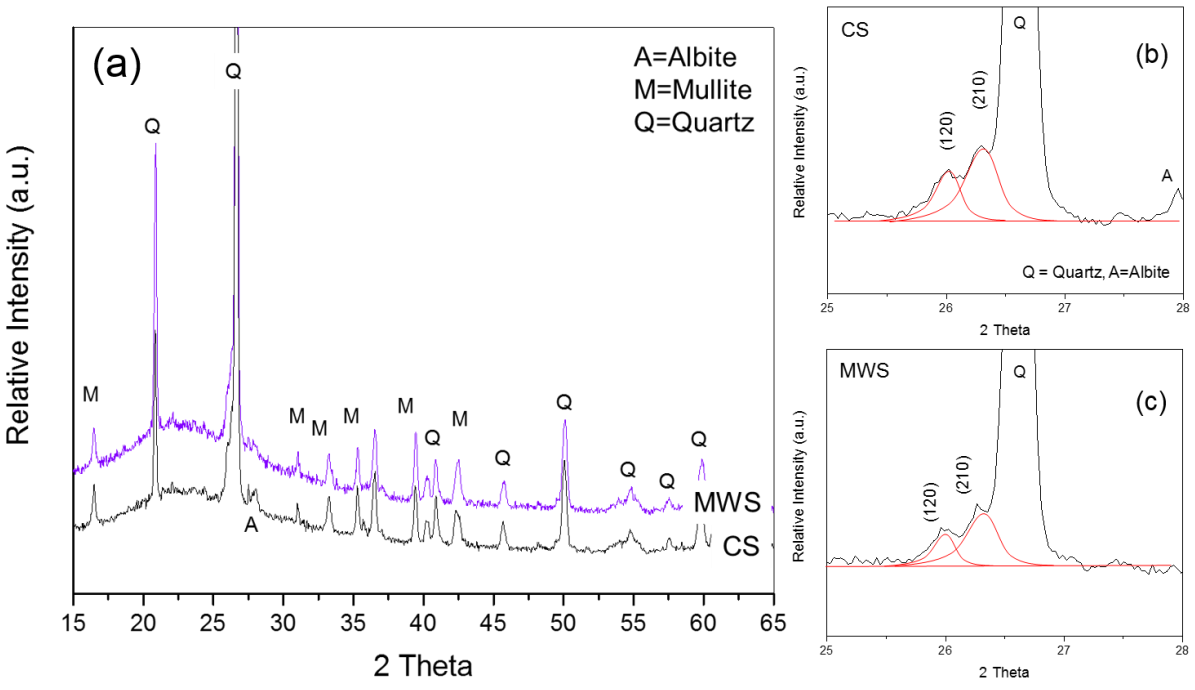

Fig. 9. a) XRD of CS and MWS porcelain samples. Mullite formed under both conditions is identified as orthorhombic mullite by the split of (120) and (210) peaks revealed in b) CS, and c) MWS.

Conclusions

Porcelain samples were fully sintered using microwave radiation at 1000 °C, a temperature 175 °C lower than when using a conventional sintering process. Liquid started to form at ~800 °C under microwave radiation while ~950 °C is required using conventional sintering. Mullite, moreover, formed under microwave radiation had small crystallite size (76 nm) but high aspect ratio (>30:1) compared to mullite from the conventional process. Mullite chemistry in both samples was slightly different; the microwave sintered samples had higher alumina content (~63 mol%) while conventionally sintered samples had stoichiometric mullite (~60 mol%). Both mullites, however, had orthorhombic crystal structure. Formation of mullite was enhanced by microwave energy and may also arise via a vapour -liquid- solid mechanism.

Acknowledgements

W. Lerdprom acknowledges Imperial College London funding no. MMRE_PG54200. A. Borrell acknowledges the Spanish Ministry of Economy and Competitiveness for her Juan de la Cierva-Incorporación contract (IJCI-2014-49839).

References

1. K.E. Haque, Microwave energy for mineral treatment processes—a brief review, *International Journal of Mineral Processing*, 57(1) (1999)1-24.

2. J.D. Katz, Microwave sintering of ceramics, *Annual Review of Materials Science*, 22(1) (1992) 153-170.

3. D.E. Clark, D.C Folz, What is microwave processing?, in D.E. Clark, D.E. Folz, C.E. Folgar, M.M.Mahmoud (Eds.), Microwave solutions for ceramics engineers, The American Ceramic Society, Westerville, Ohio, 2005, pp. 1-32.

4. R.R. Menezes, P.M. Souto, R.H. Kiminami, Microwave fast sintering of ceramic materials, in A. Lakshmanan (Ed.), Sintering of ceramics-new emerging techniques, Intech Open Access Publisher, 2012, pp.1-25.

5. V. M. Kenkre, L. Skala, M. W. Weiser, J. D. Katz, Theory of microwave interactions in ceramic materials: the phenomenon of thermal runaway, *Journal of Materials Science*, 26(9) (1991) 2483-2489.

6. J. Wang, J. Binner, B. Vaidhyanathan, N. Joomun, J. Kilner, G. Dimitrakis, T.E. Cross, Evidence for the microwave effect during hybrid sintering, *Journal of the American Ceramic Society*, 89(6) (2006)1977-1984.

7. G. Gaustad, J. Metcalfe, H. Shulman, S. Allan, Susceptor investigation for microwave heating applications, in Innovative Processing and Synthesis of Ceramics, Glasses and Composites VIII: Proceedings of the 106th Annual Meeting of the American Ceramic Society, Indianapolis, Indiana, 2005, pp. 25-35.

8. H. Shulman, M. Fall, S. Allan. Microwave assist technology for product improvement and energy efficiency. in 4th Korea/Japan International Symposium on Material Science and Resources Recycling, Jeju, South Korea, 2007, pp.142-146.

9. D.E. Clark, W.H. Sutton, Microwave processing of materials, *Annual Review of Materials Science*, 26(1) (1996) 299-331.

10. W.E. Webb, R.H. Church, Measurement of dielectric properties of minerals at microwave frequencies, Report of Investigations No. 9035, United State Bureau of Mines, 1986, pp.1-8.

11. W.M. Carty, U. Senapati, Porcelain—Raw materials, processing, phase evolution, and mechanical Behavior. *Journal of the American Ceramic Society*, 81(1) (1998) 3-20.

12. Y. Iqbal, W.E. Lee, Microstructural evolution in triaxial porcelain. *Journal of the American Ceramic Society*, 83(12) (2000) 3121-3127.

13. W. Lerdprom, Firing of porcelain, MS. Thesis, New York State College of Ceramics at Alfred University, Alfred, NY, 2014.

14. Y. Iqbal, W.E. Lee, Fired porcelain microstructures revisited. *Journal of the American Ceramic Society*, 82(12) (1999) 3584-3590.

15. R.R.Menezes, P.M. Souto, R.H. Kiminami, Microwave hybrid fast sintering of porcelain bodies, *Journal of Materials Processing Technology*, 190 (1–3) (2007) 223-229.

16. L.N. Satapathy, Microwave assisted sintering of high voltage porcelain material and its characterization, *Journal of Ceramic Processing Research*, 10(5) (2009) 637-642.

17. S. Allan, M. Fall, H. Shulman, G. Carnahan, Microwave assist sintering of porcelain insulators with large cross section, paper presented at the 33rd International Conference and Exposition on Advanced Ceramics and Composites, FL, 2009. Retieved from http://www.ceralink.com/sites/default/files/ MicrowaveAssistSintering ofPorcelainInsulatorswithLargeCross-section.pdf

18. T. Santos, L.C. Costa, L. Hennetier, M.A. Valente, J. Monteiro, J. Sousa, Microwave processing of porcelain tableware using a multiple generator configuration, *Applied Thermal Engineering*, 50(1) (2013) 677-682.

19. J. Monteiro, M. A. Valente, T. Santos, L. C. Costa, J. Sousa, Microwave radiation: An alternative method to sinter utilitarian porcelain, in Microwave & Optoelectronics Conference (IMOC), 2011 SBMO/IEEE MTT-S International, Natal, 2011, 561-564.

20. R. Benavente, M.D. Salvador, F.L. Peñaranda-Foix, O. García-Moreno, A. Borrell, High thermal stability of microwave sintered low-ε_r β-eucryptite materials, *Ceramics International*, 41(10) (2015) 13817-13822.

21. R. Benavente, A. Borrell, M.D. Salvador, O. Garcia-Moreno, F.L. Peñaranda-Foix, J.M. Catala-Civera, Fabrication of near-zero thermal expansion of fully dense β-eucryptite ceramics by microwave sintering, *Ceramics International*, 40(1) (2014) 935-941.

22. W. Lerdprom, R.K. Chinnam, D.D. Jayaseelan, W.E. Lee, Porcelain production by direct sintering, *Journal of the European Ceramic Society*, 36(16) (2016) 4319-4325.

23. V. Miceli, B. Cioni, A. Lazzeri, Microwave processing of liquid phase sintered alumina, in Proceeding of Materials Science & Technology 2009 Conference and Exhibition, Pittsburgh, PA, 2009, 50-61.

24. P. Hartman, W.G. Perdok, On the relations between structure and morphology of crystals. I. *Acta Crystallographica*, 8(1) (1955) 49-52.

25. T. Ban, K. Okada, Structure refinement of mullite by the Rietveld method and a new method for estimation of chemical composition, *Journal of the American Ceramic Society*, 75(1) (1992) 227-230.

26. M. Panneerselvam, K.J. Rao, Novel microwave method for the synthesis and sintering of mullite from kaolinite, *Chemistry of Materials*, 15(11) (2003) 2247-2252.

27. C.G. Bergeron, S. H. Risbud. Introduction to phase equilibria in ceramics, Wiley-American Ceramic Society, Ohio, USA,1986.

28. B.R. Johnson, W.M. Kriven, J. Schneider, Crystal structure development during devitrification of quenched mullite, *Journal of European Ceramics Society*, 21(14) (2001), 2541-2562.

29. B. Sonupalak, M. Sarakaya, I.A. Aksay, Spinel phase formation during the 980°C exothermic reaction in the kaolinite-to-mullite reaction series, *Journal of American Ceramic Society*, 70(11) (1987), 837-842.

30. C. Cerecedo, V. Valcárcel, M. Gómez, I. Drubi, F. Guitián, New massive vapor-liquid-solid deposition of α-Al_2O_3 fibers, *Advance Engineering Materials*, 9(7) (2007) 600–603.

31. L. Dan, Y. Xiumin, C. Jian, J. Fang, Y. Yong, H. Zhengren, L. Xuejian, Microstructure and reaction mechanism of SiC ceramic with mullite-zircon as a new liquid-phase sintering additives system, *Materials Science and Engineering: A*, 559, (2013) 510-514.